Peer-reviewed version available at Water 2017, 9, 910; doi:10.3390/w9120910

Article

Evolution of the uranium isotopic compositions of the groundwater and rock in the sandy-clayey aquifer

Alexander I. Malov*

Federal Center for Integrated Arctic Research of Russian Academy of Sciences; malovai@yandex.ru

* Correspondence: malovai@yandex.ru; Tel.: +7-911-571-7172

Abstract: Uranium isotopes actively investigated as mechanistic or time scale tracers of natural processes. This paper describes the occurrence and redistribution of U in the Vendian aquifer of the paleo valley at NW Russia. Forty-four rock samples were collected from boreholes, and twenty-five groundwater samples. The U, Fe concentration, and $^{234}U/^{238}U$ activity ratio were determined in the samples. We estimated the ^{14}C and ^{234}U-^{238}U residence time of groundwater in an aquifer. It has been established that the processes of chemical weathering of Vendian deposits led to the formation of a strong oxidation zone, developed above -250 m.a.s.l. The inverse correlation between the concentrations of uranium and iron is a result of removal of U from paleo valley slopes in oxidizing conditions and accumulation of U at the bottom of the paleo valley in reducing conditions, and accumulation of Fe on the slopes and removal from bottom. Almost all U on the slopes replaced by a newly formed hydrogenic U with a higher $^{234}U/^{238}U$ activity ratio. After that dissolution and desorption of hydrogenic U was occurred from the slopes during periods without any glaciations and marine transgressions. Elevated concentrations of U preserved in not oxidized lenses at the paleo valley bottom.

Keywords: aquifer, rock, radioactive isotopes, groundwater dating

1. Introduction

Uranium isotopes actively investigated as mechanistic or time scale tracers of natural processes [1,2]. They may have application to determine the radiological suitability of groundwater for drinking purposes [3-6], ore bodies exploration [7-9], assisting in understanding historical climates [10-12]. This justified the interest in uranium redistribution in the Vendian siltstones of the Northern Dvina Basin (NDB) – paleo valley at NW Russia (Fig. 1).

2. Materials and Methods

Study object is the Padun aquifer of the NDB. Sediments of the Padun Formation of the study area were accumulated in the coastal marine environment. The Padun Formation of the Vend 90-170-m-thick located above -150 m.a.s.l. is composed of siltstones and sandstones with intercalations of mudstones. The rocks are characterized by reddish brown color on the NDB slope and with light green lenses and spots under central part of the NDB (at the NDB bottom). Forty-four rock samples were collected from nine boreholes, and twenty-five groundwater samples (Fig. 1, Tables 1, 2).

Preprints (www.preprints.org) | NOT PEER-REVIEWED | Posted: 4 October 2017 doi:10.20944/preprints201710.0024.v1

Peer-reviewed version available at Water 2017, 9, 910; doi:10.3390/w9120910

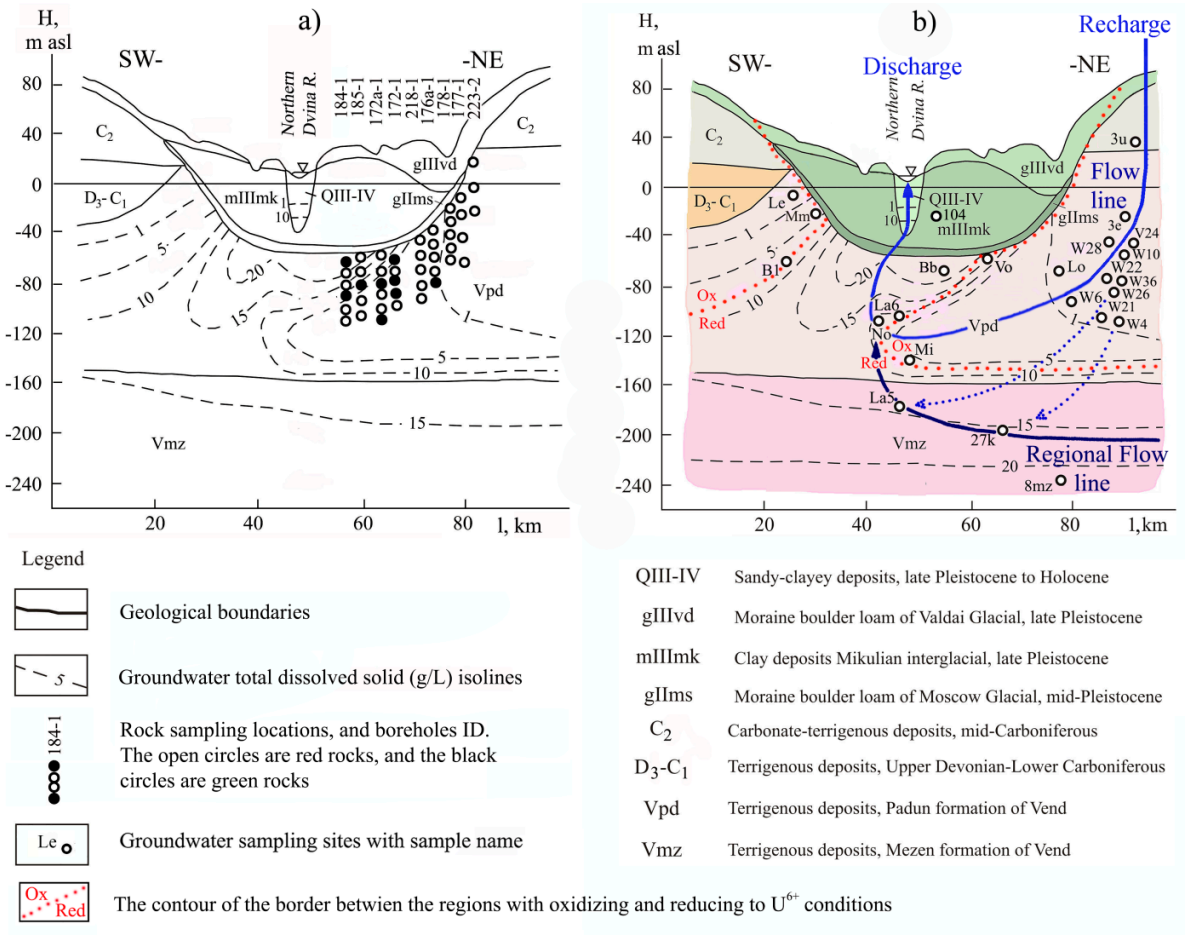

Figure 1. General location of the study site showing the rock sampling locations (a) and the groundwater sampling locations (b) on a conceptual schematic cross section of the groundwater system perpendicular to the main axis of the Northern Dvina Basin from the recharge area to the discharge in the river valley, including the location of the flow path of the water body in the aquifer.

The water temperature, pH, Eh, DO, alkalinity, total dissolved solids (TDS), Fe concentrations (C_{Fe}^{W}), U concentrations (C_{U}^{W}), $^{234}U/^{238}U$ activity ratio (AR^{W}), ^{14}C, $\delta^{13}C$ were determined in the groundwater, as described by Malov [13]. The U content (C_{U}^{R}), $^{234}U/^{238}U$ activity ratio (AR^{R}), Fe content (C_{Fe}^{R}) in rock samples were determined, as described by Malov et al. [14]. We used the piston flow model to estimate the ^{14}C residence time of groundwater in an aquifer. This model takes into account both the exchange occurs predominantly between soil CO_2 and HCO_3^-, and the exchange occurs predominantly between HCO_3^- and solid carbonate minerals [15]. We also used the mass-balance model [13,16] and model of the down-flow radioactive decay of ^{234}U excess in solution [17] to estimate the ^{234}U-^{238}U residence time of groundwater in an aquifer under oxidizing and reducing conditions for U, respectively.

3. Results and Discussion

On the NDB slope groundwater (Fig.2b, d) with Eh from -68 to 106 mV, pH from 7.7 to 9.1 and alkalinity from 1.0 to 5.2 meq/L represents fresh water. The residence time this water in aquifer ranged from 0.3 to 16.4 ka. Accordingly very low C_{Fe}^{W} (4-203, average 41 ppb), medium AR^{W} (1.3-5.9, average 3.0) and high C_{U}^{W} (0.3-12.5, average 5.4 ppb) are characteristic of this waters. At the

NDB bottom, around the redox barrier old salt water with residence time ranging from 17 to 33 ka, TDS from 4 to 13 g/L, Eh from -38 to 2 mV, pH from 7.4 to 7.8 and alkalinity from 1.7 to 4.2 meq/L is located. The maximum C_U^W (7.2-15.4, average 12 ppb), and high AR^W (4.8-7.2, average 5.9) and C_{Fe}^W (0.4-1.9, average 0.8 ppm) are observed here. Behind the redox barrier exist the oldest (^{234}U-^{238}U age from 0.1 to 0.5 Ma) and the most salty (TDS from 9 to 22 g/L) waters. The Eh ranged from -23 to -151 mV, pH ranged from 7.6 to 9, alkalinity ranged predominantly from 0.2 to 0.9 meq/L. The minimum C_U^W (0.1-1.4, average 0.4 ppb) and maximum C_{Fe}^W (0.7-8, average 3.7 ppm) are observed here. AR^W decrease from 7.16±0.94 to 2.97±0.45.

Table 1. Uranium content and $^{234}U/^{238}U$ activity ratio in the rocks of the Vendian (Ediacaran) Padun (Vpd) Formation at the Northern Dvina Basin (NDB)

Well ID	Rock[a]	Depth (m)	^{238}U (ppm)	$^{234}U/^{238}U$	Well ID	Rock	Depth (m)	^{238}U (ppm)	$^{234}U/^{238}U$
Samples taken from rocks under the central part of the NDB (NDB Bottom)					Samples taken from rocks on the slope of the NDB (NDB Slope)				
184-1	GSi	106.0	3.15±0.33	0.65±0.10	218-1	RSi	72.8	1.02±0.19	1.12±0.19
	RSi	116.4	1.13±0.22	1.17±0.17		RM	82.5	1.26±0.21	1.19±0.20
	RSi	127.2	1.92±0.36	1.09±0.15		RSa	89.4	1.16±0.18	1.23±0.21
	GSi	127.2	20.9±3.52	0.54±0.08		RSi	108.1	0.63±0.11	1.07±0.18
	RSi	143.2	0.86±0.15	1.21±0.18		RSi	114	0.81±0.14	1.34±0.21
	RSi	156.0	0.63±0.11	1.14±0.16	176a-1	RSa	68.5	1.01±0.16	1.50±0.25
185-1	RSi	122.8	0.80±0.14	1.21±0.18		RSi	72.1	1.70±0.26	1.13±0.19
	RSi	133.0	0.68±0.11	0.81±0.12		RSi	85.6	1.69±0.25	1.02±0.18
	GM	144.1	1.52±0.28	1.03±0.15		RM	97.0	1.20±0.19	1.26±0.20
	VSi	153.4	2.16±0.37	1.21±0.18		GM	97.0	3.45±0.48	1.18±0.19
	RSi	160.0	0.11±0.03	0.99±0.15	177-1	RSS	52.0	0.58±0.12	1.30±0.21
172a-1	RSS	110.6	0.76±0.13	0.99±0.15		RSi	60.8	1.03±0.16	1.33±0.22
	VSi	120.0	1.11±0.22	1.30±0.19		RSi	78.1	1.79±0.27	1.17±0.19
	GSi	133.6	4.96±0.75	1.21±0.18		RM	89.0	1.26±0.21	1.07±0.18
	RSi	133.6	1.14±0.23	1.12±0.16	178-1	RSi	72.5	1.50±0.23	1.07±0.18
	RSi	150.9	1.45±0.27	1.18±0.17		RSa	79.4	1.74±0.27	1.17±0.19
	GSi	150.9	14.9±2.31	0.77±0.11		RSi	83.0	0.85±0.15	1.21±0.21
172-1	GSi	114.0	1.46±0.23	1.07±0.15		RSa	92.0	1.73±0.27	1.13±0.18
	RSi	119.6	1.57±0.25	0.97±0.15		RSa	101.5	0.84±0.15	1.25±0.20
	GSi	119.6	3.11±0.38	0.93±0.14	223-2	RSi	49.0	2.89±0.78	1.51±0.25
	GSi	131.6	2.10±0.35	0.90±0.14		RSi	70.0	0.83±0.15	1.16±0.19
	RSi	145.0	1.11±0.22	1.12±0.16		RSi	92.0	1.01±0.17	1.05±0.17
Average			3.07±0.50	1.03±0.16	Average			1.36±0.23	1.20±0.20
Total average ^{238}U = 2.22±0.36 ppm, $^{234}U/^{238}U$ = 1.12±0.18									
Green rock average ^{238}U = 6.17±0.99 ppm, $^{234}U/^{238}U$ = 0.92±0.15									
Red rock average ^{238}U = 1.20±0.20 ppm, $^{234}U/^{238}U$ = 1.16±0.19									

[a] GSi - green siltstones, RSi – red siltstones, GM – green mudstones, RM – red mudstones, VSi - variegated siltstones, RSS – red siltstone-sandstone, RSa - red sandstones

70 **Table 2.** Measured values of the chemical and isotopic compositions of the groundwater and the calculated values of the $^{14}C_0$ and ^{14}C ages, and U age (modified after
71 Malov, 2016)

Sample name	TDS (mg/L)	pH	DO (mg/L)	T°C	^{14}C (pmc)	$\delta^{13}C$ (‰)	Age (ka)	Eh (mV)	Alkalinity (meq/L)	Fe (µg/L)	C_8^W (ppb)	AR_t
72 Samples taken from groundwater under the central part of the NDB (NDB Bottom)												
8 mz^{2014}	22,246	7.6	0	6.7	0	7.6	460±70^b	*NA*	0.16	8097	0.2±0.004	2.97±0.45
27^{2012}	15,724	7.9	1.1	5.9	*NA*	*NA*	160±25^c	-23	0.92	826	1.39±0.03	5.45±0.81
La5^{2012}	15,158	9	0	6.8	*NA*	*NA*	110±17^c	-151	0.15	6031	0.12±0.002	6.19±0.93
La6^{2012}	9065	8.4	0.3	6.3	*NA*	*NA*	90±15^c	- 42	0.7	708	0.47±0.01	6.53±0.98
No^{2014}	8954	8.3	1.2	6.8	0	*NA*	80±14^c	-82	0.57	1352	0.28±0.01	6.72±1.05
Bb^{2003}	20,619	*NA*	*NA*	*NA*	*NA*	*NA*	*NA*	*NA*	3.97	400	*NA*	*NA*
B1^{2012}	8399	7.7	1.2	5.7	5.78±0.24	-16.6	27.3±0.6^a	-38	4.18	1872	15.22±0.3	5.46±0.82
B1^{2014}	9193	7.6	*NA*	5.8	5.79±0.19	-15.6	26.1±0.6^a	*NA*	4.07	776	15.38±0.3	5.41±0.81
Vo^{2012}	13,370	7.7	0	5.3	*NA*	*NA*	22.2±3.3^b	*NA*	2.18	*NA*	13.84±0.3	4.75±0.71
Mi^{2014}	5317	7.4	0	5	1.70±0.26	-14.6	33.0±2.3^a	-25	1.74	439	9.86±0.2	7.16±0.94
MM^{2012}	4362	7.8	*NA*	4.8	*NA*	*NA*	16.6±2.4^b	2	3.75	443	7.24±0.14	6.4±0.96
73 Samples taken from groundwater on the slope of the NDB (NDB Slope)												
3e^{2015}	138	8.7	3.5	4.8	34.18±0.59	-12.3	2.1±0.3^a	-68	1.62	203	12.15±0.24	2.26±0.34
W10^{2014}	387	9.1	1.4	4.1	*NA*	*NA*	11.7±1.8^b	101	3.67	5.6	11.22±0.22	2.39±0.36
W6^{2014}	738	8.9	0.6	4.5	25.30±0.64	-9.6	4.0±0.3^a	99	3.75	9.5	5.21±0.92	2.86±0.42
W21^{2014}	647	8.6	2.9	4.6	*NA*	*NA*	4.8±0.8^b	23	3.44	18.2	7.55±0.15	1.99±0.3
W4^{2012}	638	9	0	4.7	*NA*	*NA*	16.4±2.4^b	106	3.97	3.9	7.0±0.14	4.76±0.72
V24^{2012}	307	8.6	1.5	3.8	*NA*	*NA*	8.9±1.4^b	-12	3.33	71.9	5.71±0.11	3.51±0.52
3u^{2014}	285	7.7	*NA*	4.0	44.97±1.08	-8.7	1.3±0.2^b	*NA*	3.21	65.7	4.01±0.84	1.46±0.22
3u^{2015}	93	7.8	*NA*	4.9	*NA*	*NA*	*NA*	*NA*	1.02	94.9	0.25±0.01	1.28±0.21
W22^{2014}	383	8.4	1.2	4.1	24.86±0.43	-10.1	4.6±0.4^a	-8	3.02	14.3	6.37±0.13	1.63±0.24
W28^{2014}	260	8.2	3.3	3.9	58.40±0.89	-11.0	2.0±0.3^b	106	3.05	9.3	2.99±0.06	2.39±0.36

W26[2014]	365	8.1	0.8	4.4	*NA*	*NA*	2.8±0.4[b]	-34	3.61	10.8	2.38±0.05	3.04±0.45
W36[2014]	348	8.2	2.7	5.2	25.01±0.47	-11.7	5.8±0.4[a]	-62	3.56	59.1	2.0±0.04	4.81±0.62
Lo[2014]	790	9.0	1.8	4.7	37.03±0.67	-11.2	5.4±0.8[b]	NA	5.25	26.4	1.78± 0.04	5.94± 0.84
Le[2012]	209	8.2	6	5	51.67±0.63	-11.5	0.3±0.05[b]	-24	2.61	165	1.70±0.03	1.43±0.21

NA not analyzed; *NC* not calculated

[a] ^{14}C age, [b] ^{234}U-^{238}U age, [c] ^{234}U-^{238}U age of the regional and local flow systems mix groundwater (see Fig.1)

Preprints (www.preprints.org) | NOT PEER-REVIEWED | Posted: 4 October 2017 doi:10.20944/preprints201710.0024.v1

Peer-reviewed version available at Water 2017, 9, 910; doi:10.3390/w9120910

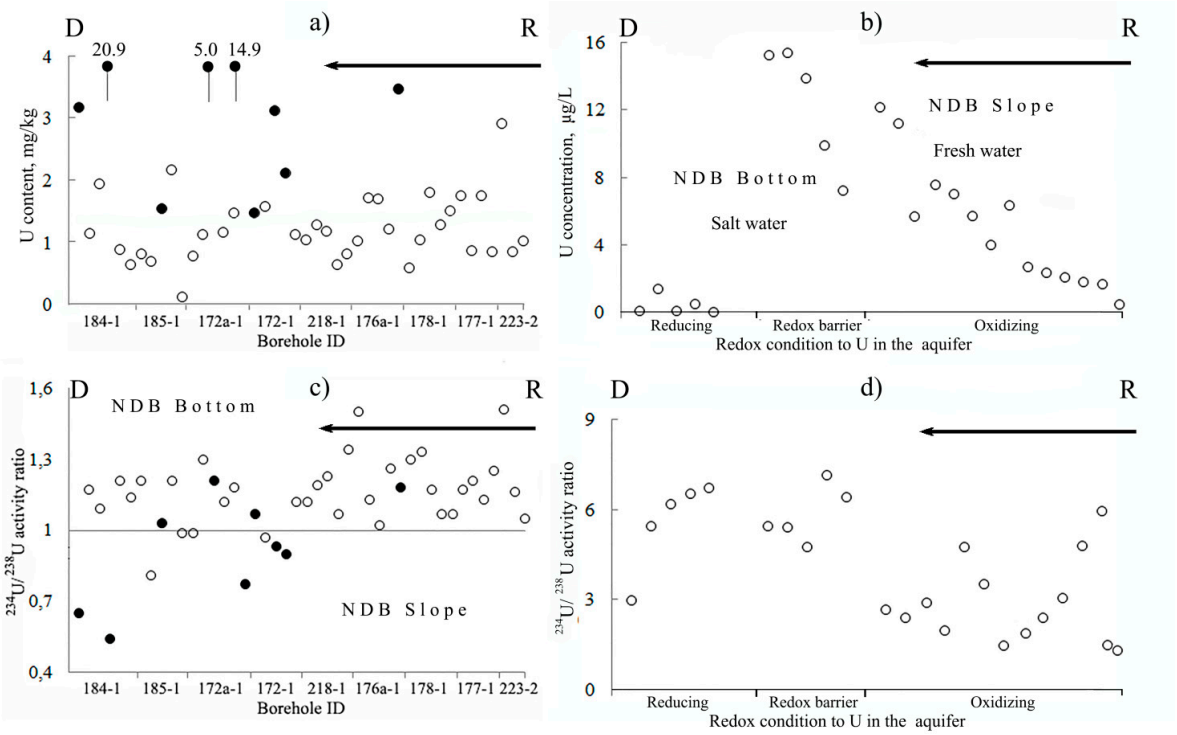

Figure 2. Uranium and its isotopes distribution in Padun aquifer of the NDB from the recharge on the watershed («R» on the graphs) to the NDB slope and NDB bottom and discharge in the river valley («D» on the graphs): red (empty circles) and green (solid circles) rock samples (a, c) and groundwater samples (b, d). Arrows indicate the direction of groundwater flow path and uranium redistribution.

Behind the redox barrier, the uranium changed to U^{4+} speciation and precipitates, its concentration in rocks reach 20 ppm, $^{234}U/^{238}U$ activity ratio in rocks decreases to 0.5-0.9 (Fig.2a, c). However, total precipitation does not occur because the process of recoil loss continues and ^{238}U enters into the water with ^{234}U. For every 1 atom of ^{234}U in rock, ~18,000 atoms of ^{238}U exist; therefore, recoil atoms inevitably encounter and knock other atoms from the crystal lattice, creating an area of disorder. The uranium atoms in the disordered zone are first transferred to water, resulting in a disturbance of the radioactive equilibrium in the water. Evidence that recoil atoms are not transferred into water alone but carry away a certain amount of ^{238}U atoms explains why AR^W under reducing conditions usually does not exceed 10-20. This is possible if 1000-2000 ^{238}U atoms are transferred into the water for every recoil atom.

The maximum AR^W in groundwater directly close to the barrier is estimated to be 8.1 (sample Mi^{2014}). In other samples, the activity ratio is lower, namely, from 6.72±1.05 to 2.97±0.45, which suggests a greater age for the groundwater in these samples, in accordance with a simple model of the down-flow radioactive decay of excess ^{234}U in solution.

$C_U{}^R$ in the red rock ranged from 0.11 ppm to 2.89 ppm, average 1.2 ppm. $C_U{}^R$ in the green rock ranged from 1.52 ppm to 20.9 ppm, average 6.17 ppm. AR^R in the red rock ranged from 0.87 to 1.51, average 1.16. AR^R in the green rock ranged from 1.18 to 0.54, average 0.92 ppm. The average value of $C_U{}^R$ on the slope of the NDB is 1.36 ppm, AR^R is 1.2; at the bottom of the NDB average values are 3.07 and 1.03, respectively.

The average value of C_{Fe}^{R} from 18 samples of red rocks on the slope of the NDB is 3.67%. In two samples from wells 184-1 on the NDB bottom C_{Fe}^{R} in the red rock is 2.33%, C_{Fe}^{R} in the green rock is 1.83%.

In Upper Vendian products of the rocks weathering were transferred to the study area with nearby eastern tip of the Baltic Shield and were deposited together with the buried organic matter. In subsequent geological periods (Upper Devonian-Lower Carboniferous) NDB was also in coastal marine and lake environment under hot humid climate [18,19]. In such anoxic environments, early diagenesis conditions favor the reduction of U^{6+} into low solubility U^{4+}, which decreases U concentrations in overlying waters and sediment pore-waters [20]. This period was the most favorable for the supergene ore formation [21,22]. During these periods, apparently, and was the main flow of uranium to the study area and its deposition as a result of hydrolysis, adsorption on natural sorbents and changes oxidizing conditions of the environmental in reducing conditions.

Transgressive period, in Middle Carboniferous-Permian led to the formation of a cover of the terrigenous-carbonate deposits, however, during the long continental environmental interspace in the Mesozoic-Pliocene was formed the NDB palaeo valley. Its depth could reach 250-300 meters. The depth of the valley and its Pliocene age are confirmed by the data of other paleovalleys of the East European platform [23-25]. Within its boundaries, most of the Palaeozoic sediments were destroyed, and Vendian deposits were brought to the surface.

The processes of chemical weathering of Vendian deposits led to the formation a strong oxidation zone, developed above -250 m.a.s.l. Deeper increased proportion of Fe^{2+} iron, is typical presence of bitumen, organic carbon, pyrite, and rock kept the gray-green color [26,27]. During this period, probably occurred main redistribution of uranium accumulated in the Paleozoic in the Padun aquifer of the NDB. The inverse correlation between the concentrations of uranium and iron is typical for Padun rock (see above). It is a result of removal of U from NDB slopes in oxidizing conditions and accumulation of U at the bottom of the NDB in reducing conditions, and accumulation of Fe on the slopes and removal from bottom. As a result, significant part of the equilibrium U on the slopes of the NDB had been replaced by a newly formed hydrogenic U with an initial $AR_0 \approx AR^W$ of modern fresh groundwater = 3, and the initial U concentration of the rocks $C_0^R \approx C_U^R$ of modern siltstones of the region (2.6 ppm). Ending of the period of co-precipitation of hydrogenic uranium with iron hydroxide on NDB slopes can be estimated from the following equation [17]:

$$t_1 = \lambda_4^{-1} \ln\left[(AR_0 - 1)(AR_t - 1)^{-1}\right],$$

where λ_4 – decay constant for $^{234}U = 2.8263 \cdot 10^{-6}$ (a^{-1}) [28]; AR_t – average AR^R of red rock = 1.16.

We get: t_1 = 0.9 Ma, which should roughly correspond to the period of a sharp cold snap in the region and filling of the paleo valley by clay material [29-32]. The duration of the subsequent removal of hydrogenic uranium from the NDB slopes can be estimated from the following equation [13]:

$$t_2 = (C_8^W \cdot R)(R_d \cdot M_s \cdot C_8^R)^{-1},$$

where C_8^W – concentration of U was passed from the red siltstones to the water for a time t ($C_0^R - C_U^R$) = (2.6 – 1.2) = 1.4 ppm; M_s – solid mass to fluid unit volume ratio = 9.2; C_8^R – average concentration of U in solid phase for a time t: ($C_0^R + C_U^R$):2 = 1.9 ppm; R:p = 24; and average R_d:p = $3.6 \cdot 10^{-6}$ a^{-1}.

We get: t_2 = 0.5 Ma. The difference ($t_1 - t_2$) should roughly correspond to the duration of glaciations and marine transgressions in the past 0.9 Ma, when the movement of groundwater in the Padun aquifer was significantly delayed or even absent [33-36]. Removal of uranium was not appeared, but radioactive decay was continued.

Lower values of AR^R in the green siltstones can be explained by the fact that these deposits have reached a steady state AR_U that depends only on their size (AR_U = 0.92, the average grain size $d_p \approx$ 30 μm) [37], because were under reducing conditions over 1 Ma. Significantly higher content of uranium in them compared to red siltstones show considerable variability into the permeability values of the aquifer, whereby they were away from the paths of groundwater filtration and have retained uranium. A similar situation is typical for the preserved here iodine water lens (sample Bb^{2003}), the source which are the iodine-containing seaweed from the Mikulinian interglacial Boreal sea.

4. Conclusions

The processes of chemical weathering of Vendian deposits led to the formation of a strong oxidation zone, developed above -250 m.a.s.l. The inverse correlation between the concentrations of uranium and iron is a result of removal of U from NDB slopes in oxidizing conditions and accumulation of U at the bottom of the NDB in reducing conditions, and accumulation of Fe on the slopes and removal from bottom. Almost all the U on the slopes of the paleo valley could be replaced by a newly formed hydrogenic U with a higher $^{234}U/^{238}U$ activity ratio. After that dissolution and desorption of hydrogenic U was occurred from the slopes of paleo valley during periods without any glaciations and marine transgressions. Elevated concentrations of U preserved in not oxidized lenses at the NDB bottom.

Acknowledgments: This work was supported by the Federal Agency of Scientific Organizations (project no. 0410-2014-0032).

References

1. Porcelli, D. Investigating groundwater processes using U- and Th-series nuclides. *Radioact. Environ.* **2008.** *13*, 105-153.
2. Baskaran M. (Ed). *Handbook of Environmental Isotope Geochemistry*. Springer: Berlin-Heidelberg, Germany, 2011.
3. Dhaoui, Z., Chkir, N., Zouari, K., Hadj Ammar, F., Agoune, A. Investigation of uranium geochemistry along groundwater flow path in the Continental Intercalaire aquifer (Southern Tunisia). *J Environ. Radioactiv*. **2016**. *157*, 67-76.
4. Wang, F., Tan, L., Liu, Q., Li, R., Li, Z., Zhang, H., et al. Biosorption characteristics of Uranium (VI) from aqueous solution by pollen pini. *J Environ. Radioactiv*. **2015.** *150*, 93-98
5. Yi, Z. Yao, J, Chen, H-l, Wang, F, Yuan, Z., Liu, X., Uranium biosorption from aqueous solution onto *Eichhornia crassipes*. *J Environ. Radioactiv.* **2016.** *154*, 43-51.
6. Manickum, T., John, W., Terry, S., Hodgson, K. Preliminary study on the radiological and physicochemical quality of the Umgeni Water catchments and drinking water sources in KwaZulu-Natal, South Africa. *J Environ. Radioactiv.* **2014.** *137*, 227-240.

7. Hall, S.M., Mihalasky, M.J., Tureck, K.R., Hammarstrom, J.M., Hannon, M.T. Genetic and grade and tonnage models for sandstone-hosted roll-type uranium deposits, Texas Coastal Plain. *Ore Geology Reviews*, **2017.** *80*, 716-753.
8. Cuvier, A., Panza, F., Pourcelot, L., et al. Uranium decay daughters from isolated mines: Accumulation and sources. *J Environ. Radioactiv*. **2015.** *149*, 110-120.
9. Keatley, A.C., Scott, T.B., Davis, S., Jones, C.P., Turner, P. An investigation into heterogeneity in a single vein-type uranium ore deposit: Implications for nuclear forensics. *J Environ. Radioactiv*. **2015.** *150*, 75-85.
10. Dosseto, A., Schaller, M. The erosion response to Quaternary climate change quantified using uranium isotopes and in situ-produced cosmogenic nuclides. *Earth-Science Rev*. **2016.** *155*, 60-81.
11. Jamieson, R.A., Baldini, J.U.L., Brett, M.J., et al. Intra- and inter-annual uranium concentration variability in a Belizean stalagmite controlled by prior aragonite precipitation: A new tool for reconstructing hydro-climate using aragonitic speleothems. *Geochim. Cosmochim. Acta* **2016**. 190, 332-346.
12. Wang, Q., Song, J., Li, X., Yuan, H., Li, N., Cao, L. Environmental evolution records reflected by radionuclides in the sediment of coastal wetlands: A case study in the Yellow River Estuary wetland. *J Environ. Radioactiv*. **2016.** *162-163*, 87-96.
13. Malov, A.I. Estimation of uranium migration parameters in sandstone aquifers. *J Environ. Radioactiv*. **2016.** *153*, 61-67.
14. Malov, A.I., Bolotov, I.N., Pokrovsky, O.S. et al. Modeling past and present activity of a subarctic hydrothermal system using O, H, C, U and Th isotopes. *Appl. Geochem.* **2015.** *63*, 93-104.
15. Han, L.F., Plummer, N. A review of single-sample-based models and other approaches for radiocarbon dating of dissolved inorganic carbon in groundwater. *Earth-Science Rev.* **2016.** *152*, 119-142.
16. Malov, A.I. The use of the geological benchmarks to assess the residence time of groundwater in the aquifer using uranium isotopes on the example of the Northern Dvina basin. *Lithol. Miner. Resour*. **2013.** *48*, 254-265.
17. Ivanovich, M., Fröhlich, K., Hendry, M.J. Uranium-series radionuclides in fluids and solids, Milk River aquifer, Alberta, Canada. *Appl. Geochem.* **1991**. *6*, 405-418.
18. Grazhdankin, D.V., Podkovyrov, V.N., Maslov, A. V. Paleoclimatic Environments of the Formation of Upper Vendian Rocks on the Belomorian-Kuloi Plateau, Southeastern White Sea Region. *Lithol. Miner. Resour.* **2005.** *40*, 232-244
19. Rozanov, A.Yu., Bessonova, V.Ya., Brangulis, A.P., Giants, V.A. *Paleogeography and lithology of the Vendian and Cambrian of the western part of the Eastern European Platform*. Nauka: Moscow, Russia, 1980 (in Russian).
20. Barnes, C.E., Cochran, J.K. Uranium geochemistry in estuarine sediments: controls on removal and release processes. *Geochim. Cosmochim. Acta* **1993**. *57*, 555-589.
21. Mikhailov, B.M. (Ed). *The forecast of the supergene zones at solid minerals.* VSEGEI: St. Petersburg, Russia, 1998 (in Russian).
22. Shore, G.M., Starchenko, V.V., Myronyuk, E.P. et al. *Requirements to maps of the ore-bearing of the supergene zones*. VSEGEI: St. Petersburg, Russia, 2005 (in Russian).
23. Goretsky, G.I. *Alluvium of the great anthropogenic paleorivers of the Russian Plain*. Nauka: Moscow, Russia, 1964 (in Russian).
24. Kashtanov, S.G. The geological data of Pliocene age of the Kazanka and Sviyaga rivers valleys. *Uchenye Zapiski Kazanskogo Universiteta* **1954**. *114*, 155-163 (in Russian).
25. Kashtanov, S.G. New data to the history of the Paleo-Kama. *Dokl. Earth Sci*. **1956.** *106*, 708-711.

26. Malov, A.I. Water-Rock Interaction in Vendian Sandy-Clayey Rocks of the Mezen Syneclise. *Lithol. Miner. Resour.* **2004.** *39,* 345-356.
27. Zverev, V.P., Malov, A.I., Kostikova, I.A. Geochemical state groundwater of the active water exchange zone at the Lomonosov diamond deposit. *Geoecology* **2005.** *4,* 298-303 (in Russian).
28. Cheng, H., Edwards, R.L., Hoff, J. et al. The half-lives of uranium-234 and thorium-230. *Chem. Geol.* **2000.** *169*, 17-33.
29. Head, M.J., Gibbard, P.L. Early-Middle Pleistocene transitions: Linking terrestrial and marine realms. *Quatern. Int.* **2015**. *389*, 7-46.
30. Azzaroli, A., De Giuli, C., Ficcarelli, G., Torre, D. Late pliocene to early mid-pleistocene mammals in Eurasia: Faunal succession and dispersal events. *Palaeogeogr. Palaeoclimatol. Palaeoecol*. **1988.** *66,* 1-143.
31. Markova, A.K., Vislobokova, I.A. Mammal faunas in Europe at the end of the Early – Beginning of the Middle Pleistocene. *Quatern. Int*. **2016.** *420*, 363-377.
32. Muttonia, G., Giancarlo Scardiab, G., Kentc, D.V. Human migration into Europe during the late Early Pleistocene climate transition. *Palaeogeogr. Palaeoclimatol. Palaeoecol*. **2010.** *296*, 79-93.
33. Ehlers, J., Astakhov, V., Gibbard, P.L., Mangerud, J., Svendsen, J.I. GLACIATIONS | Middle Pleistocene in Eurasia. In *Reference Module in Earth Systems and Environmental Sciences. Encyclopedia of Quaternary Science,* 2nd ed.; Elsevier, 2013; pp. 172–179.
34. Lisitsyn, A.P. (Ed.). *The White Sea system*. Nauchn. Mir: Moscow, 2010 (in Russian).
35. Molodkov, A.N., Bolikhovskaya, N.S. Long-term palaeoenvironmental changes recorded in palynologically studied loess–palaeosol and ESR-dated marine deposits of Northern Eurasia: Implications for sea–land correlation. *Quatern. Int.* **2006.** *152–153*, 37–47.
36. Glaznev, V.N., Kukkonen, I.T., Rajewsky, A.B., Ekinen, J. New data on the heat flow in the central part of the Kola Bay. *Dokl. Earth Sci*. **2004.** *396*, 102-104.
37. DePaolo, D.J., Maher, K., Christensen, J.N. et al. Sediment transport time measured with U-series isotopes: Results from ODP North Atlantic drift site 984. *Earth Planet. Sci. Lett.* **2006**. *248,* 394-410.